Polymer 255 (2022) 125167

Contents lists available at ScienceDirect

Polymer

journal homepage: www.elsevier.com/locate/polymer

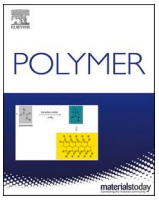

Elastic modulus of polyamide thin films formed by molecular layer deposition

Olivia M. McIntee [a,b,*], Brian C. Welch [a,b], Alan R. Greenberg [a,b], Steven M. George [c], Victor M. Bright [a]

[a] Department of Mechanical Engineering, University of Colorado, Boulder, CO, 80309, USA
[b] Membrane Science, Engineering and Technology (MAST) Center, University of Colorado, Boulder, CO, 80309, USA
[c] Department of Chemistry, University of Colorado, Boulder, CO, 80309, USA

ARTICLE INFO

Keywords:
Molecular layer deposition
Atomic force microscopy
Elastic modulus
Polyamide thin films

ABSTRACT

Molecular layer deposition (MLD) is a gas-phase deposition technique that can create ultra-thin films with precisely controlled chemical composition and thickness by depositing one monolayer at a time. This makes MLD an attractive technology for desalination membranes among other applications. Given its relatively recent development, little information has been reported regarding the properties of MLD thin films. We present the results of an initial mechanical property study of MLD films with thicknesses ranging from ~50 to 2000 nm. MLD was utilized to create crosslinked polyamide films grown using either *m*-phenylenediamine (MPD) and trimesoyl chloride (TMC) reactants or piperazine (PIP) and TMC reactants. The elastic modulus of the films was determined using atomic force microscopy (AFM). The results show that the modulus was independent of film thickness with values of 4.36 ± 1.19 GPa and 5.24 ± 1.06 GPa for the MLD films grown using the MPD-TMC and PIP-TMC chemistries, respectively. These values are of the same order of magnitude as those reported for much thicker polyamide films, but higher than the modulus of polyamide films fabricated using interfacial polymerization.

1. Introduction

The mechanical properties of polymeric membranes are important considerations in the continuing effort for improved material performance. Thin film composite (TFC) membranes, typically comprised of a thin, dense polyamide layer atop a much thicker, porous polymeric support, remain the most often used membrane material in reverse osmosis (RO) desalination. TFCs must withstand deformation during the assembly and long-term operation of high-pressure spiral-wound membrane modules [1,2]. To reduce membrane resistance and decrease operating costs the selective dense layer should be as thin and homogeneous as possible [3–5]. However, as the surface-to-volume ratio of thin films and ultra-thin films increases, the characteristics of the substrate-film and film-air interfaces have greater effects on their mechanical behavior [6–8]. Therefore, future development of TFC membranes with improved transport properties must be coupled with a better understanding of the mechanical characteristics of the ultra-thin selective layer to avoid plastic deformation or failure of the film [1,9].

The thin polyamide films utilized in the subject study were fabricated using molecular layer deposition (MLD). MLD is an analogous process to atomic layer deposition (ALD) and is an ultra-thin film deposition technique that uses sequential, self-limiting reactions to produce conformal and uniform films (Fig. 1) [10,11]. Under vacuum, a sample is exposed to reactive precursors one at a time to build up a film with Angstrom-scale precision. In the first step, the surface is exposed to the first precursor. The functional groups of this reactant (e.g., an acyl chloride) form a covalent bond with the surface through a polycondensation (or similar) reaction. Subsequently, the precursor and reaction byproducts are purged away. At this point, a monolayer has developed on the surface which now has the functionality of the first precursor (acyl chloride). During the second step, the sample is exposed to another precursor with a new functional group (e.g., an amine). Once again, a monolayer of material is covalently bonded to the surface whose functionality, once more, changes. After a second purge, the process may be repeated to increase the film thickness.

The mechanical properties of MLD films have been sparsely studied.

* Corresponding author. Department of Mechanical Engineering, University of Colorado, Boulder, CO, 80309, USA.
E-mail addresses: olivia.mcintee@colorado.edu (O.M. McIntee), bwelch@colorado.edu (B.C. Welch), alan.greenberg@colorado.edu (A.R. Greenberg), steven.george@colorado.edu (S.M. George), victor.bright@colorado.edu (V.M. Bright).

https://doi.org/10.1016/j.polymer.2022.125167
Received 6 May 2022; Received in revised form 12 July 2022; Accepted 14 July 2022
Available online 18 July 2022
0032-3861/

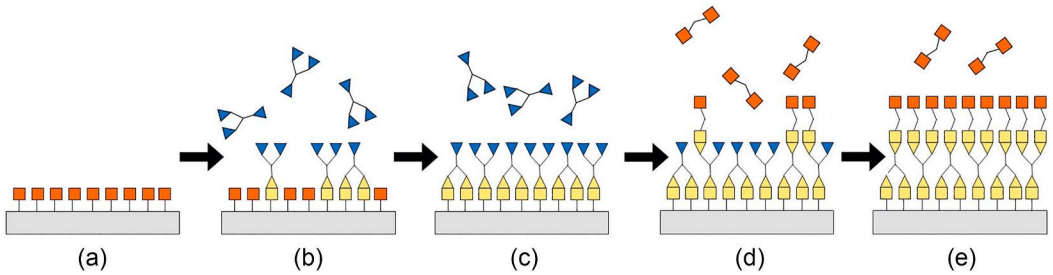

Fig. 1. MLD process: (a) Original surface is exposed to the first reactant (blue), and (b) surface sites are saturated with the reactant, generating a surface with new functional groups; (c) excess reactant is purged from the chamber with inert gas, and (d) new functional groups on the surface are exposed to the second reactant (orange), (e) reactive sites are saturated, and after purging, provide a surface ready for repeat reaction cycles. (For interpretation of the references to color in this figure legend, the reader is referred to the Web version of this article.)

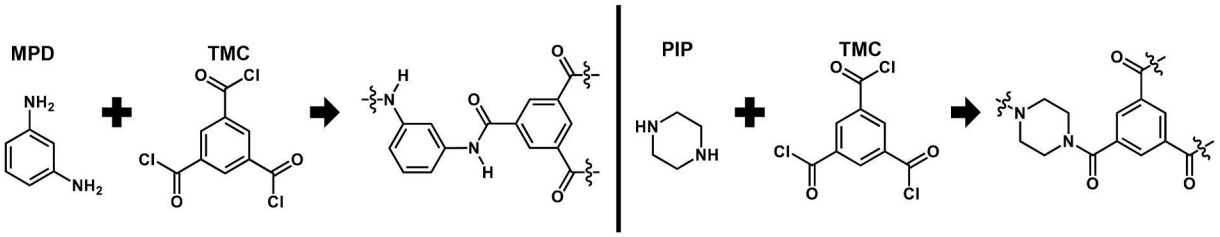

Fig. 2. The two chemistries used in the MLD process. left: *m*-phenylenediamine (MPD) and trimesoyl chloride (TMC) reactants form a fully aromatic polyamide film; right: piperazine (PIP) and TMC reactants form a semi-aromatic polyamide film.

Some studies include the modulus of organic-inorganic hybrid MLD films measured with nanoindentation [12–15]. Of particular interest is a study done by Nye et al. on polyurea MLD films [16]. Picosecond acoustic analysis was used to determine the modulus of the polyurea films and researchers used this information in addition to chemical analysis techniques to determine trends with film thickness. The differences found between the two MLD polyureas gave insight into the mechanisms of MLD film growth and morphology of the films.

One technique employed to measure the mechanical properties of thin films is atomic force microscopy (AFM). AFM enables correlation between topographic and property data at high spatial resolution [17]. Several studies have used an AFM for indentation of polymer thin films [18–22]. A newer AFM technique termed PinPoint™, operates in a contact mode where the AFM cantilever deforms the sample and collects a force-distance curve at each pixel in the image, thus measuring topographical and mechanical characteristics simultaneously. Given its reported advantages [23–25], AFM PinPoint™ was chosen to investigate the modulus of the thin polymer films used for this study.

The two polyamide MLD films in this study have been used to fabricate RO membranes and to improve the mechanical characteristics of battery electrodes [26–28]. One is a fully aromatic polyamide made using *m*-phenylenediamine (MPD) and trimesoyl chloride (TMC) reactants and the other is a semi-aromatic polyamide made using piperazine (PIP) and TMC reactants (Fig. 2). The focus of this study is to investigate the influence of film thickness and chemistry on the elastic modulus of these polyamide MLD films. The work expands the literature regarding the mechanical properties of MLD films and provides an improved basis for advanced polymer film engineering for technologies such as membranes, batteries, and flexible electronics.

2. Experimental

2.1. Film fabrication

A rotating spatial reactor was used to deposit the MLD films as shown in Fig. S1 of the supplementary information. The reactor had an inner drum that rotated samples between two exposure zones. The volumes between the exposure zones served as purging zones. A single rotation of the inner drum corresponded to a single MLD cycle. Exposure and purge times could be altered by changing the rotation speed. Film thickness could be varied by changing the number of cycles. More details on the design and operation of this system were provided in Refs. [29,30].

The two polyamide chemistries shown in Fig. 2 were utilized for the MLD films, which were grown on silicon substrates. MLD film samples of desired thickness were fabricated in the spatial MLD reactor using a temperature of 115 or 130 °C and a rotation speed of 20 or 120 RPM.

Film thickness was measured using spectroscopic ellipsometry (J.A. Woollam Co., Inc., M − 2000).

2.2. Atomic force microscopy

Mechanical property measurements of the MLD films were obtained with an atomic force microscope (AFM) (NX10, Park Systems Corp., Suwon, Korea). The AFM measurements were performed in PinPoint™ mode whereby the AFM cantilever deforms the sample and collects a force-distance curve at each pixel in the image. A representative force-separation curve is shown in Fig. S2 of the supplementary information. The cantilever selected was SD-R30-NCH (Nanosensors, Neuchatel, Switzerland) with a spring constant of 42 N/m, resonance of 330 kHz, and a tip radius of 30 nm ± 10 nm. A spring constant calibration step was performed with the Sader method, which takes into account the specific geometry of the cantilever measured by optical microscopy [31, 32].

Each scan image is 5 × 5 μm with a resolution of 256 × 256 pixels. All AFM measurements were recorded at ambient conditions. Force-distance curves were taken at an approach and retract speed of 10 μm/s. Each sample was scanned 2–3 times in randomly chosen areas except the 48 nm MPD-TMC sample, which only includes a single measurement scan.

To calculate an accurate modulus value the contact area between the probe tip and the sample surface must be known [33–36]. PinPoint™ mode requires a minimum deformation of 1 nm to create reliable contact between the probe tip and sample surface. This minimum deformation was chosen as the selection criteria for reliable AFM scans. The

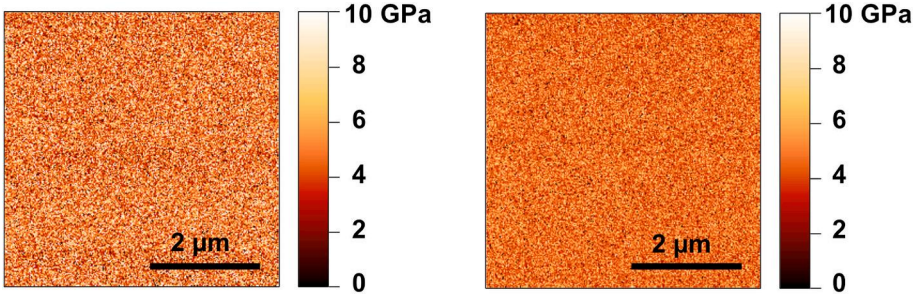

Fig. 3. Representative 5 × 5 μm AFM modulus scans of MLD films on silicon substrates. Left: a 225 nm thick MPD-TMC film with a mean modulus of 5.4 GPa; right: 260 nm thick PIP-TMC MLD film with a mean modulus of 4.8 GPa. (For interpretation of the references to color in this figure legend, the reader is referred to the Web version of this article.)

uniformity of the AFM images was monitored to avoid tip wear and contamination effects. To better quantify tip contamination, the adhesion force was also monitored from the force-distance curves [37]. To avoid artifacts, a maximum adhesion force threshold of 50 nN was utilzed for the measurements.

A bare silicon chip was measured to obtain the RMS roughness of the silicon substrate. An OMCL-AC160TS (Olympus Corporation, Tokyo, Japan) cantilever with a spring constant of 26 N/m, resonance of 300 kHz, and tip radius of 7 nm was used in non-contact mode for this purpose. Two random 5 × 5 μm areas were probed to measure the RMS roughness.

2.3. Elastic modulus calculation

The modulus at each pixel was calculated using the Johnson-Kendall-Roberts (JKR) model [35]. The JKR model uses points on the unloading segments from the force-separation curve to calculate the modulus (Fig. S3). Using a Poisson's ratio, υ, of 0.4 [38] and tip radius, R, of 30 nm, Equation (1) from the JKR model can be used to calculate the elastic modulus, E [25,39,40]:

$$E = \frac{3}{4}\left(1-\upsilon^2\right)\left(\frac{1+16^{1/3}}{3}\right)^{3/2}\frac{F_1}{\left(R\left(d_0-d_1\right)^3\right)^{1/2}} \quad (1)$$

The values of d_0, d_1, and F_1 were taken from the force-separation curve, such as the force-separation curve in Fig. S3, where d is the separation distance of the probe and F is the force.

2.4. Image processing

The AFM images were processed using the open source Gwyddion software (version 2.60). To better visualize the data and obtain a more accurate mean modulus value, extreme pixels had to be removed with a mask. Pixels with a modulus value greater than three standard deviations from the mean were excluded from the data set because it was determined that the AFM had performed a poor-quality indent. A poor-quality indent could be due to sample or probe contamination. This occurred in less than 2% of the pixels. The extremely high modulus values from these pixels were orders of magnitude higher than what the AFM could accurately measure. Additionally, such a range in properties is not expected for the homogeneous MLD films. This procedure was applied to all AFM PinPoint™ modulus scans. Standard statistical analysis was used to calculate the mean and standard deviation of the AFM measurements.

3. Results and discussion

3.1. MLD film modulus

MPD-TMC and PIP-TMC MLD films with thicknesses ranging from ~50 to 2300 nm and ~100 to 1200 nm, respectively, were characterized using AFM PinPoint™ mode. To validate the measurement technique, a poly(methyl methacrylate) (PMMA) film was fabricated and measured using the same protocol as the MLD films. The mean modulus from three AFM scans was measured as 3.12 ± 0.19 GPa. This mean modulus is in the range for bulk values reported in literature for PMMA films (2.6–4.2 GPa) [41,42]. Other recent studies have used PinPoint™ mode to measure the mechanical properties of bulk and thin film polymers [23–25]. Representative AFM modulus images of MLD films are shown in Fig. 3. It is important to note that each image indicates a uniform modulus by the unvarying coloration. This speaks to the excellent homogeneity of MLD thin film mechanical properties.

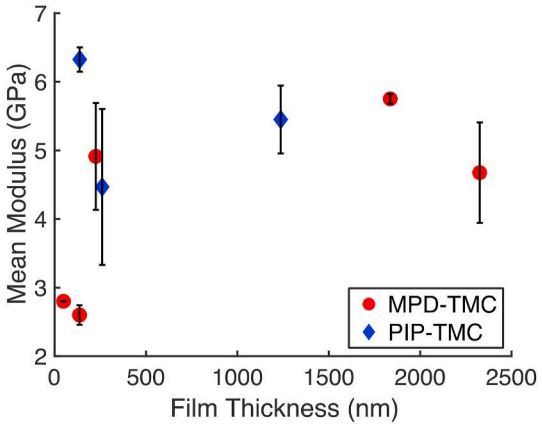

Fig. 4. Collective modulus measurements of all MLD films with respect to film thickness. Each point represents the mean modulus and standard deviation calculated from a 2–3 AFM scans. Samples were remeasured at randomly chosen locations.

In addition, topography measurements indicated that the MLD films were conformal and smooth. All MLD samples had an RMS roughness less than 1 nm. When a bare silicon substrate was measured in non-contact mode, the RMS roughness of two 5 × 5 μm images (256 × 256 pixels) were 1.49 nm and 0.99 nm. Thus, the MLD films did not increase the roughness of the substrate.

The full set of MLD mean moduli are shown in Fig. 4. Overall, the modulus values ranged from ~2.6–5.8 GPa for the MPD-TMC films and ~4.5–6.3 GPa for the PIP-TMC films. Statistical analysis of the data was conducted to evaluate the dependence of modulus on film thickness. Neither of the chemistries evidenced a statistically significant result. However, the two thinnest MPD-TMC films measured have a smaller modulus than the other films. To help eliminate the possibility of a measurement artifact, subsequent measurements of the 2300 nm MPD-TMC sample were made, and the initial mean modulus value of 4.7 GPa was confirmed. In addition, it is important to note that low values were not observed for the PIP-TMC film of comparable thickness.

Table 1
Comparison of polyamide film modulus values reported in the literature using various fabrication and measurement techniques.

Film Fabrication Technique	Chemistry	Measurement Method	Modulus [GPa]	Reference
MLD	MPD-TMC	AFM	4.36	This work
MLD	PIP-TMC	AFM	5.24	This work
IP	MPD-TMC	AFM	0.55, 0.90	[24]
IP	MPD-TMC	Film wrinkling	0.10–2.71	[3]
IP	PIP-TMC	Film wrinkling	0.25	[3]
IP	MPD-TMC	Film wrinkling	1.4	[48]
IP	PIP-TMC	Film wrinkling	1.3	[48]
Extrusion	Hexamethylenediamine - Adipic acid	AFM	2.54	[22]
Injection	Hexamethylenediamine - Isophthalic acid	AFM	3.49	[22]

The literature reports that thin film moduli can increase [7,41,45], decrease [8,43,44], or remain the same as the film thickness decreases [6,41]. One challenge in measuring thin films is the influence that instrumentation may have on observed values and trends. For example, Nguyen et al. found that an AFM probe with a larger radius was more prone to measure substrate effects than probes with a smaller radius for the same film thicknesses [39]. To successfully analyze thickness dependent trends in thin films, the probe contact area must be lesser than the size effects of the free sample surface [45–47]. In the present study there were no observed systematic changes in modulus due to influence from the substrate or the AFM probe.

The samples were then analyzed in terms of film chemistry. The mean and standard deviation for the collective MPD-TMC and PIP-TMC samples were 4.45 ± 1.21 GPa and 5.28 ± 1.09 GPa, respectively. Analysis indicated no statistically significant difference which matches other findings for MPD-TMC and PIP-TMC films measured at room temperature [3,48].

3.2. Comparison of MLD film moduli to interfacial polymerized film moduli

The overall mean modulus of the MPD-TMC and PIP-TMC MLD films is higher than those reported in literature for polyamide films fabricated through interfacial polymerization (IP), the most common commercial technique for fabricating polymer RO membranes (Table 1). IP is a semi-self-limiting solvent-based chemical reaction that takes place when a porous support soaked in an aqueous solution containing one reactant (MPD) contacts an organic solution containing the other reactant (TMC), thus forming a thin film at the interface of the two phases. Once the film is continuous the two phases are separated, diffusion is limited, and the reaction is complete [49].

Chong and Wang fabricated thin IP polyamide films atop a porous ceramic substrate and used AFM PinPoint™ to measure the modulus of the film across the pore. Depending on the size of the pore, the reported modulus values for the film suspended over the pore ranged from 0.55 ± 0.5 GPa to 0.9 ± 0.5 GPa [24]. The authors note the possibility of substrate effects to explain the differences between the modulus values. The MLD films used in the present study were supported by a non-porous substrate and no increases in modulus were measured due to substrate effects as the film thickness decreased.

Another consideration is the roughness of the substrate. When using AFM contact mode on a rough surface, the exact contact area of the AFM probe tip is unknown, and this could produce artificially inhomogeneous modulus measurements [33]. However, in the present study the MLD films were smooth (RMS <1 nm), so surface roughness effects were unlikely, and the contact area was taken as the theoretical area of a 30 nm radius tip.

A film wrinkling technique has been employed to measure the plane strain modulus of the IP polyamide dense layer of commercial RO (TMC-MPD) and nanofiltration (PIP-TMC) membranes [48,50]. The researchers reported modulus values of 1.4 ± 0.5 GPa and 1.3 ± 0.1 GPa for the RO and nanofiltration membranes, respectively. These values were smaller than those of the MLD polyamide films reported in this study. A possible explanation could be structural differences between the MLD and IP films. Since MLD is a sequential, gas-phase deposition technique the reactions yield a film with complete crosslinking as indicated by Fourier transform infrared (FTIR) spectroscopy and x-ray photoelectron spectroscopy (XPS) studies [29]. IP films do not exhibit complete crosslinking according to XPS studies [48]. However, for polyamides measured at room temperature, well below their glass transition temperature, crosslinking should not be a meaningful source of deviation in modulus values [51,52].

Film morphology on the other hand, could impact measured modulus values. IP films contain tortuous voids and folds that make the actual film thickness difficult to measure and could produce an artificially low calculated modulus using the wrinkling wavelength technique [5,53]. In contrast, MLD films are smooth and defect-free. When Karan et al. fabricated a smooth IP film (RMS = 0.6 nm), the reported modulus was 2.71 GPa using the film wrinkling technique [3]. This value is closer to the MLD polyamide film moduli reported in the present study providing support for the possible role of film morphology in modulus measurement. Macroscale film morphology differences between the solid MLD films and the porous IP films may cause the measured modulus of the MLD films to be higher.

In addition, Cervera-Moreno et al. used AFM indentation to measure various amorphous and semicrystalline polyamides [22]. The sample thicknesses studied were on the order of 100 μm and were manufactured with extrusion and injection molding, so the properties were likely representative of a bulk material. The reported modulus values were between 1.99 and 3.49 GPa, in the same range as those reported here for the MLD films. Differences in chemical structure between the aliphatic films from Cervera-Moreno et al. [22] and the aromatic MLD films do not appear to produce a meaningful difference in modulus values. It should be noted that the use of different measurement techniques might obscure any such differences.

4. Conclusions

MLD thin films were fabricated on silicon substrates, and modulus measurements were conducted using AFM in PinPoint™ mode. The modulus was determined to be independent of thickness for both the MPD-TMC and PIP-TMC chemistries evaluated and values for the two chemistries were statistically similar. The obtained range of ~3–6 GPa was on the same order of magnitude as values reported for much thicker polyamide films, but higher than the modulus of polyamide films made with interfacial polymerization.

The uniformity of the AFM modulus images revealed the homogeneity of MLD film mechanical properties, a desirable characteristic for reliable and consistent membrane fabrication.

This is the first known study of the modulus of all-organic MLD films and provides useful data for MLD modeling and for a range of applications. A more comprehensive analysis with additional thicknesses and chemistries combined with chemical analysis techniques would provide further insights on MLD growth mechanisms and film morphology. Fabricating IP films from the same chemistries and measuring the mechanical properties to provide a baseline of comparison for MLD thin

films will be the focus of future work. This would aid in the potential expansion of MLD applications.

CRediT authorship contribution statement

Olivia M. McIntee: Conceptualization, Formal analysis, Investigation, Methodology, Visualization, Writing – original draft, Writing – review & editing. **Brian C. Welch:** Investigation, Resources, Visualization, Writing – review & editing. **Alan R. Greenberg:** Conceptualization, Writing – review & editing, Supervision, Funding acquisition. **Steven M. George:** Funding acquisition, Resources, Writing – review & editing. **Victor M. Bright:** Writing – review & editing, Supervision, Funding acquisition.

Declaration of competing interest

The authors declare that they have no known competing financial interests or personal relationships that could have appeared to influence the work reported in this paper.

Data availability

Data will be made available on request.

Acknowledgements

This research was supported by the Membrane Science, Engineering and Technology (MAST) Center (NSF IUCRC Award IIP 1624602) at the University of Colorado Boulder and a National Science Foundation Graduate Research Fellowship under Grant No. DGE 2040434. The authors thank Armando Melgarejo from Park Systems Corp. for technical guidance and Chris Buelke for PMMA film fabrication.

Appendix A. Supplementary data

Supplementary data to this article can be found online at https://doi.org/10.1016/j.polymer.2022.125167.

References

[1] E. Elele, Y. Shen, J. Tang, Q. Lei, B. Khusid, G. Tkacik, C. Carbrello, Mechanical properties of polymeric microfiltration membranes, J. Membr. Sci. 591 (2019), 117351, https://doi.org/10.1016/j.memsci.2019.117351.

[2] M. Aghajani, M. Wang, L.M. Cox, J.P. Killgore, A.R. Greenberg, Y. Ding, Influence of support-layer deformation on the intrinsic resistance of thin film composite membranes, J. Membr. Sci. 567 (2018) 49–57, https://doi.org/10.1016/j.memsci.2018.09.031.

[3] S. Karan, Z. Jiang, A.G. Livingston, Sub–10 nm polyamide nanofilms with ultrafast solvent transport for molecular separation, Science 348 (2015) 1347–1351, https://doi.org/10.1126/science.aaa5058.

[4] S.-J. Park, W. Choi, S.-E. Nam, S. Hong, J.S. Lee, J.-H. Lee, Fabrication of polyamide thin film composite reverse osmosis membranes via support-free interfacial polymerization, J. Membr. Sci. 526 (2017) 52–59, https://doi.org/10.1016/j.memsci.2016.12.027.

[5] T.E. Culp, B. Khara, K.P. Brickey, M. Geitner, T.J. Zimudzi, J.D. Wilbur, S.D. Jons, A. Roy, M. Paul, B. Ganapathysubramanian, A.L. Zydney, M. Kumar, E.D. Gomez, Nanoscale control of internal inhomogeneity enhances water transport in desalination membranes, Science 371 (2021) 72–75, https://doi.org/10.1126/science.abb8518.

[6] R.K. Bay, K. Zarybnicka, J. Jančář, A.J. Crosby, Mechanical properties of ultrathin polymer nanocomposites, ACS Appl. Polym. Mater. 2 (2020) 2220–2227, https://doi.org/10.1021/acsapm.0c00201.

[7] M. Saito, K. Ito, H. Yokoyama, Mechanical properties of ultrathin polystyrene- *b* -polybutadiene- *b* -polystyrene block copolymer films: film thickness-dependent Young's modulus, Macromolecules 54 (2021) 8538–8547, https://doi.org/10.1021/acs.macromol.1c01406.

[8] Z. Ao, S. Li, Temperature- and thickness-dependent elastic moduli of polymer thin films, Nanoscale Res. Lett. 6 (2011) 243, https://doi.org/10.1186/1556-276X-6-243.

[9] M. Aghajani, S.H. Maruf, M. Wang, J. Yoshimura, G. Pichorim, A. Greenberg, Y. Ding, Relationship between permeation and deformation for porous membranes, J. Membr. Sci. 526 (2017) 293–300, https://doi.org/10.1016/j.memsci.2016.12.048.

[10] S.M. George, Atomic layer deposition: an overview, Chem. Rev. 110 (2010) 111–131, https://doi.org/10.1021/cr900056b.

[11] P. Sundberg, M. Karppinen, Organic and inorganic–organic thin film structures by molecular layer deposition: a review, Beilstein J. Nanotechnol. 5 (2014) 1104–1136, https://doi.org/10.3762/bjnano.5.123.

[12] D.C. Miller, R.R. Foster, S.-H. Jen, J.A. Bertrand, D. Seghete, B. Yoon, Y.-C. Lee, S. M. George, M.L. Dunn, Thermomechanical properties of aluminum alkoxide (alucone) films created using molecular layer deposition, Acta Mater. 57 (2009) 5083–5092, https://doi.org/10.1016/j.actamat.2009.07.015.

[13] J.-P. Niemelä, N. Rohbeck, J. Michler, I. Utke, Molecular layer deposited alucone thin films from long-chain organic precursors: from brittle to ductile mechanical characteristics, Dalton Trans. 49 (2020) 10832–10838, https://doi.org/10.1039/D0DT02210A.

[14] B.H. Lee, B. Yoon, A.I. Abdulagatov, R.A. Hall, S.M. George, Growth and properties of hybrid organic-inorganic metalcone films using molecular layer deposition techniques, Adv. Funct. Mater. 23 (2013) 532–546, https://doi.org/10.1002/adfm.201200370.

[15] J.J. Brown, R.A. Hall, P.E. Kladitis, S.M. George, V.M. Bright, Molecular layer deposition on carbon nanotubes, ACS Nano 7 (2013) 7812–7823, https://doi.org/10.1021/nn402733g.

[16] R.A. Nye, A.P. Kelliher, J.T. Gaskins, P.E. Hopkins, G.N. Parsons, Understanding molecular layer deposition growth mechanisms in polyurea via picosecond acoustics analysis, Chem. Mater. 32 (2020) 1553–1563, https://doi.org/10.1021/acs.chemmater.9b04702.

[17] Y. Liu, I. Sokolov, M.E. Dokukin, Y. Xiong, P. Peng, Can AFM be used to measure absolute values of Young's modulus of nanocomposite materials down to the nanoscale? Nanoscale 12 (2020) 12432–12443, https://doi.org/10.1039/D0NR02314K.

[18] A.-Y. Jee, M. Lee, Comparative analysis on the nanoindentation of polymers using atomic force microscopy, Polym. Test. 29 (2010) 95–99, https://doi.org/10.1016/j.polymertesting.2009.09.009.

[19] S. Markutsya, C. Jiang, Y. Pikus, V.V. Tsukruk, Freely suspended layer-by-layer nanomembranes: testing micromechanical properties, Adv. Funct. Mater. 15 (2005) 771–780, https://doi.org/10.1002/adfm.200400149.

[20] B. Du, O.K.C. Tsui, Q. Zhang, T. He, Study of elastic modulus and yield strength of polymer thin films using atomic force microscopy, Langmuir 17 (2001) 3286–3291, https://doi.org/10.1021/la001434a.

[21] K. Miyake, N. Satomi, S. Sasaki, Elastic modulus of polystyrene film from near surface to bulk measured by nanoindentation using atomic force microscopy, Appl. Phys. Lett. 89 (2006) 31925, https://doi.org/10.1063/1.2234648.

[22] J.J. Cervera-Moreno, A. Martinez-Borquez, P. Sotta, M. Laurati, AFM investigation of the influence of ethanol absorption on the surface structure and elasticity of polyamides, SN Appl. Sci. 1 (2019) 1325, https://doi.org/10.1007/s42452-019-1360-0.

[23] I. Stoica, E.-L. Epure, C.-P. Constantin, M.-D. Damaceanu, E.-L. Ursu, I. Mihaila, I. Sava, Evaluation of local mechanical and chemical properties via AFM as a tool for understanding the formation mechanism of pulsed UV laser-nanoinduced patterns on azo-naphthalene-based polyimide films, Nanomaterials 11 (2021) 812, https://doi.org/10.3390/nano11030812.

[24] J.Y. Chong, R. Wang, From micro to nano: polyamide thin film on microfiltration ceramic tubular membranes for nanofiltration, J. Membr. Sci. 587 (2019), 117161, https://doi.org/10.1016/j.memsci.2019.06.001.

[25] S. Kim, Y. Lee, M. Lee, S. An, S.-J. Cho, Quantitative visualization of the nanomechanical Young's modulus of soft materials by atomic force microscopy, Nanomaterials 11 (2021) 1593, https://doi.org/10.3390/nano11061593.

[26] B.C. Welch, O.M. McIntee, A.B. Ode, B.B. McKenzie, A.R. Greenberg, V.M. Bright, S.M. George, Continuous polymer films deposited on top of porous substrates using plasma-enhanced atomic layer deposition and molecular layer deposition, J. Vac. Sci. Technol. 38 (2020) 52409, https://doi.org/10.1116/6.0000271.

[27] B.C. Welch, O.M. McIntee, T.J. Myers, A.R. Greenberg, V.M. Bright, S.M. George, Molecular layer deposition for the fabrication of desalination membranes with tunable metrics, Desalination 520 (2021), 115334, https://doi.org/10.1016/j.desal.2021.115334.

[28] J.M. Wallas, B.C. Welch, Y. Wang, J. Liu, S.E. Hafner, R. Qiao, T. Yoon, Y.-T. Cheng, S.M. George, C. Ban, Spatial molecular layer deposition of ultrathin polyamide to stabilize silicon anodes in lithium-ion batteries, ACS Appl. Energy Mater. 2 (2019) 4135–4143, https://doi.org/10.1021/acsaem.9b00326.

[29] D.J. Higgs, J.W. DuMont, K. Sharma, S.M. George, Spatial molecular layer deposition of polyamide thin films on flexible polymer substrates using a rotating cylinder reactor, J. Vac. Sci. Technol.: Vac. Surf. Films 36 (2018) 1A117, https://doi.org/10.1116/1.5004041.

[30] K. Sharma, R.A. Hall, S.M. George, Spatial atomic layer deposition on flexible substrates using a modular rotating cylinder reactor, J. Vac. Sci. Technol.: Vac. Surf. Films 33 (2015) 1A132, https://doi.org/10.1116/1.4902086.

[31] J.E. Sader, J.A. Sanelli, B.D. Adamson, J.P. Monty, X. Wei, S.A. Crawford, J. R. Friend, I. Marusic, P. Mulvaney, E.J. Bieske, Spring constant calibration of atomic force microscope cantilevers of arbitrary shape, Rev. Sci. Instrum. 83 (2012), 103705, https://doi.org/10.1063/1.4757398.

[32] J.E. Sader, J.W.M. Chon, P. Mulvaney, Calibration of rectangular atomic force microscope cantilevers, Rev. Sci. Instrum. 70 (1999) 3967–3969, https://doi.org/10.1063/1.1150021.

[33] D. Haba, J. Kaufmann, A.J. Brunner, K. Resch, C. Teichert, Observation of elastic modulus inhomogeneities in thermosetting epoxies using AFM – discerning facts and artifacts, Polymer 55 (2014) 4032–4040, https://doi.org/10.1016/j.polymer.2014.06.030.

[34] D. Maugis, Extension of the johnson-kendall-roberts theory of the elastic contact of spheres to large contact radii, Langmuir 11 (1995) 679–682, https://doi.org/10.1021/la00002a055.
[35] K.L. Johnson, K. Kendall, A.D. Roberts, Surface energy and the contact of elastic solids, Proc. Math. Phys. Eng. Sci. 324 (1971) 301–313, https://doi.org/10.1098/rspa.1971.0141.
[36] T.D.B. Jacobs, C. Mathew Mate, K.T. Turner, R.W. Carpick, Understanding the tip-sample contact: an overview of contact mechanics from the macro- to the nanoscale, in: D.G. Yablon (Ed.), Scanning Probe Microscopy in Industrial Applications, John Wiley & Sons, Inc, Hoboken, NJ, 2013, pp. 15–48, https://doi.org/10.1002/9781118723111.ch2.
[37] X. Yu, N.A. Burnham, R.B. Mallick, M. Tao, A systematic AFM-based method to measure adhesion differences between micron-sized domains in asphalt binders, Fuel 113 (2013) 443–447, https://doi.org/10.1016/j.fuel.2013.05.084.
[38] James E. Mark, 43. Nylon 6,6, in: Polymer Data Handbook, second ed., Oxford University Press, 2009, pp. 263–284, 2nd ed. https://app.knovel.com/hotlink/pdf/id:kt006PVM03/polymer-data-handbook/nylon-6-6.
[39] H.K. Nguyen, S. Fujinami, K. Nakajima, Elastic modulus of ultrathin polymer films characterized by atomic force microscopy: the role of probe radius, Polymer 87 (2016) 114–122, https://doi.org/10.1016/j.polymer.2016.01.080.
[40] Y. Sun, B. Akhremitchev, G.C. Walker, Using the adhesive interaction between atomic force microscopy tips and polymer surfaces to measure the elastic modulus of compliant samples, Langmuir 20 (2004) 5837–5845, https://doi.org/10.1021/la036461q.
[41] J. Chang, K.B. Toga, J.D. Paulsen, N. Menon, T.P. Russell, Thickness dependence of the Young's modulus of polymer thin films, Macromolecules 51 (2018) 6764–6770, https://doi.org/10.1021/acs.macromol.8b00602.
[42] M.F. Pantano, C. Pavlou, M.G. Pastore Carbone, C. Galiotis, N.M. Pugno, G. Speranza, Highly deformable, ultrathin large-area poly(methyl methacrylate) films, ACS Omega 6 (2021) 8308–8312, https://doi.org/10.1021/acsomega.1c00016.
[43] C.M. Stafford, B.D. Vogt, C. Harrison, D. Julthongpiput, R. Huang, Elastic moduli of ultrathin amorphous polymer films, Macromolecules 39 (2006) 5095–5099, https://doi.org/10.1021/ma060790i.
[44] J.M. Torres, C.M. Stafford, B.D. Vogt, Impact of molecular mass on the elastic modulus of thin polystyrene films, Polymer 51 (2010) 4211–4217, https://doi.org/10.1016/j.polymer.2010.07.003.
[45] C.A. Tweedie, G. Constantinides, K.E. Lehman, D.J. Brill, G.S. Blackman, K.J. Van Vliet, Enhanced stiffness of amorphous polymer surfaces under confinement of localized contact loads, Adv. Mater. 19 (2007) 2540–2546, https://doi.org/10.1002/adma.200602846.
[46] H.K. Nguyen, S. Fujinami, K. Nakajima, Size-dependent elastic modulus of ultrathin polymer films in glassy and rubbery states, Polymer 105 (2016) 64–71, https://doi.org/10.1016/j.polymer.2016.10.012.
[47] J. Peanasky, L.L. Cai, S. Granick, C.R. Kessel, Nanorheology of confined polymer melts. 3. Weakly adsorbing surfaces, Langmuir 10 (1994) 3874–3879, https://doi.org/10.1021/la00022a078.
[48] J.-H. Lee, J.Y. Chung, E.P. Chan, C.M. Stafford, Correlating chlorine-induced changes in mechanical properties to performance in polyamide-based thin film composite membranes, J. Membr. Sci. 433 (2013) 72–79, https://doi.org/10.1016/j.memsci.2013.01.026.
[49] F. Zhang, J. Fan, S. Wang, Interfacial polymerization: from chemistry to functional materials, Angew. Chem. Int. Ed. 59 (2020) 21840–21856, https://doi.org/10.1002/anie.201916473.
[50] J.Y. Chung, J.-H. Lee, K.L. Beers, C.M. Stafford, Stiffness, strength, and ductility of nanoscale thin films and membranes: a combined wrinkling–cracking methodology, Nano Lett. 11 (2011) 3361–3365, https://doi.org/10.1021/nl201764b.
[51] J.E. Mark (Ed.), Polymer Data Handbook, second ed., Oxford University Press, Oxford ; New York, 2009.
[52] S.H. Maruf, D.U. Ahn, A.R. Greenberg, Y. Ding, Glass transition behaviors of interfacially polymerized polyamide barrier layers on thin film composite membranes via nano-thermal analysis, Polymer 52 (2011) 2643–2649, https://doi.org/10.1016/j.polymer.2011.04.022.
[53] S. Habib, S.T. Weinman, A review on the synthesis of fully aromatic polyamide reverse osmosis membranes, Desalination 502 (2021), 114939, https://doi.org/10.1016/j.desal.2021.114939.